Suboptimal Class DE Operation for Ultrasound Transducer Arrays

Carlos Christoffersen, Thinh Ngo, Ruiqi Song, Yushi Zhou, Samuel Pichardo, Laura Curiel
Department of Electrical Engineering
Lakehead University
Thunder Bay, ON, P7B 5E1, Canada
Email: cchristo, tngo, rsong1, yzhou30, spichard, lcuriel@lakeheadu.ca

***Abstract*—Recently, integrated class DE amplifiers without matching networks have been proposed as a compact solution to drive piezoelectric ultrasound transducers for high-intensity focused ultrasound (HIFU) therapy. However, when driving a transducer array, it is not always possible to drive all transducers in ideal Class DE conditions due to variations in the impedance of each array element. This paper outlines a method to predict switching losses and to select good driving parameters for an entire array without using matching networks. To the best of the authors knowledge, this is the first paper to present such a method. The method is experimentally validated using an integrated driver developed by the authors.**

I. Introduction

Recently [1], [2], integrated drivers based on class DE amplifiers have been proposed as a compact solution to drive piezoelectric ultrasound transducers for high-intensity focused ultrasound (HIFU) therapy. Frequently HIFU operation is guided by Magnetic Resonance Imaging (MRI) [3], which provides high contrast volumetric information and real-time monitoring of thermal effects. A multi-element ultrasound transducer array is required in order to electronically steer the focal zone. Most existing transducer drivers require matching networks that interfere with the MRI-guidance system [1]. These drivers can only be used if they are placed several meters away from the magnet using individual transmission lines to connect to each transducer. This increases the complexity and ultimately the cost of HIFU equipment. As a result, there is a need for a driving system that can pilot a large number of elements, with enough power, at high efficiency, and must be compatible with an MRI environment. When driving a transducer array, due to variations in the impedance of each array element, it is usually not possible to simultaneously drive all transducers in the ideal conditions determined in [1]. Moreover, some transducers may not even admit ideal Class DE driving conditions. This paper presents a method to determine the driver parameters and predict load power and switching losses in each amplifier.

II. System Modelling and Analysis

A. Transducer Array

The six transducers used in this work are made of piezo-composite crystal (DL47, DeL Piezo, West Palm Beach, FL) and shaped as a disc with a diameter of 7 mm and a thickness of 2.8 mm. For the purpose of amplifier tuning only the part of the equivalent circuit corresponding to the fundamental resonance is considered, as shown in Fig. 1. The impedance of the series resonant branch is denoted $Z_S = R_S + jX_S$. Transducer parameters are temperature-dependent and they also change with the acoustic environment. In order to consider variations in the acoustic environment, two characterizations were performed for each transducer: one with absorber material perpendicular to the transducer (Table I) and another with the absorber material at an angle of 45° respect to the transducer (Table II). The series and parallel resonance frequencies are denoted f_s and f_p, respectively.

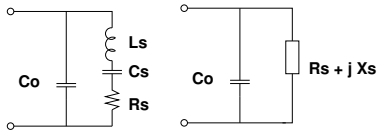

Fig. 1. Piezoelectric transducer simplified equivalent circuit.

TABLE I
Transducer parameters perpendicular absorber

Transducer	1	2	3	4	5	6
f_S (kHz)	1054	1055	1055	1056	1056	1054
f_p (kHz)	1077	1080	1084	1081	1087	1077
C_0 (pF)	95	96	86	66	117	99
R_S (Ω)	615	443	718	743	562	417

TABLE II
Transducer parameters 45° absorber

Transducer	1	2	3	4	5	6
f_S (kHz)	1055	1055	1060	1052	1056	1055
f_p (kHz)	1077	1081	1084	1081	1087	1079
C_0 (pF)	95	96	80	87	123	80
R_S (Ω)	623	454	696	806	589	418

B. Suboptimal Class DE Amplifier Analysis

Fig. 2 shows a simplified schematic diagram of a class DE amplifier. The parallel capacitor

$$C_p = C_0 + C_{SW} + C_{ext} \ ,$$

includes the transducer parallel capacitor (C_0), the parasitic capacitance of the switches (C_{SW}) and any additional external

capacitance (C_{ext}). If optimum Class DE switching conditions are not possible, we relax zero voltage switching (ZVS) while still enforcing zero derivative switching (ZDS). This is illustrated in Fig. 3. The duty cycle (D) is defined as follows:

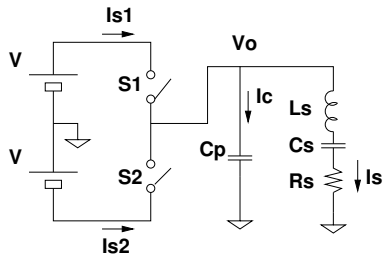

Fig. 2. Simplified schematic of a class DE amplifier.

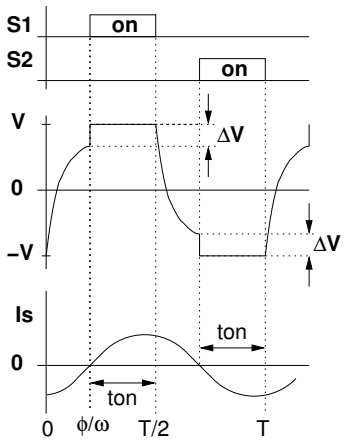

Fig. 3. Waveforms in class DE amplifier outside optimum conditions.

$$D = \frac{t_{on}}{T} \ ,$$

where t_{on} is the conduction time. The switches are operated with a duty cycle between 0 and 0.5, usually close to 0.25. The conduction angle (ϕ) is related to D:

$$\phi = \pi(1 - 2D) \ .$$

The voltage difference at the switch at the turn-on instant is denoted as ΔV. The energy loss (E_S) due to suboptimal switching is given by:

$$E_S = \frac{1}{2} C_p \Delta V^2 \ .$$

The average power switching loss (P_S) is thus estimated as follows:

$$P_S = \frac{C_P}{T} \Delta V^2 = f C_p \delta^2 V^2 \ , \tag{1}$$

where $T = 1/f$ is the period of the excitation and $\delta = \Delta V / V$.

The operation of the Class DE amplifier outside optimum conditions has been analyzed before [6] and more recently the effect of nonlinear capacitances has also been studied [7]. In this section we show a simpler set of equations for the special case where the load is a piezoelectric transducer. Following similar steps as shown in [5], but considering the waveforms shown in Fig. 3, the condition for ZDS operation is given by:

$$\omega C_p R_S = \frac{1 - \cos(2\phi) + \delta\left(\frac{3}{2} + \frac{\cos(2\phi)}{2} - 2\cos\phi\right)}{(2-\delta)\pi} \tag{2}$$

$$\omega C_p X_s = \frac{2\phi - \sin(2\phi)}{2\pi} \ , \tag{3}$$

where ω is the angular frequency. These equations are consistent with Equation (5) in [5] when $\delta = 0$. The average power dissipated at the load (P_L) is:

$$P_L = \frac{1}{2} R_S \left(\frac{(2-\delta)\omega C_p V}{1 - \cos\phi} \right)^2 \ . \tag{4}$$

III. Determination of Driving Parameters

For the following steps we assume that the minimum switch and external capacitances (C_{SW} and C_{ext}) are known and are the same for all transducer drivers, but C_0 may vary for each transducer.

1) Calculate the impedance of the series resonance branch at the frequency of operation:
$$Z_S = \frac{1}{\frac{1}{Z_T} - j\omega C_0} \ ,$$
where Z_T is the measured transducer impedance.
2) For each frequency in the range considered, numerically solve for ϕ for each transducer in (3) and use that value to solve for δ from (2):
$$\delta = \begin{cases} \frac{2\pi\omega C_p R_S - 1 + \cos(2\phi)}{\pi\omega C_p R_S + \frac{3}{2} + \frac{\cos(2\phi)}{2} - 2\cos\phi} & \text{if } \delta \geq 0 \\ 0 & \text{otherwise} \end{cases}$$
If $\delta < 0$ it is possible to increase the external capacitance C_{ext} to make $\delta = 0$. The value of C_{ext} is obtained by solving for C_p and ϕ in (2) and (3) with $\delta = 0$. For this reason, a negative value is equivalent to zero switching losses for this optimization process. Fig. 4 shows the values of D for all transducers in the frequency range where suboptimal Class DE operation is possible.
3) Calculate the overall array efficiency (η) as a function of frequency using (1) and (4):
$$\eta = \frac{\sum_i P_{Li}}{\sum_i P_{Li} + P_{Si} + P_{Oi}} \ , \tag{5}$$
and find the maximum. Here, the i subscript represents the transducer index and P_O accounts for other driver losses, mainly gate driver and switch resistance losses. The duty cycle for each transducer at a given frequency is retrieved from the result of the previous step.

Fig. 5 shows the array efficiency for different values of P_O. For this array, there are points of maximum efficiency in this frequency range for $P_O \leq 60$ mW. For large values of P_O the overall efficiency goes down and switching losses become a less important factor. Assuming P_O is known for a given driver the operating frequency could be selected near the corresponding maximum point and D for each driver is obtained from Fig. 4. Table III lists the calculated parameters for each transducer at $f = 1069$ kHz.

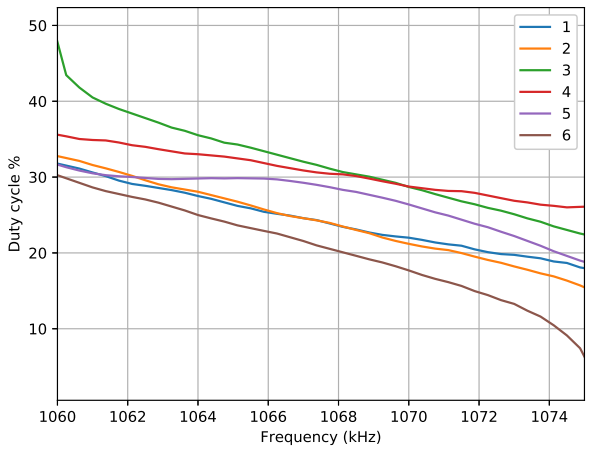

Fig. 4. Optimum duty cycle as a function of frequency for all transducers in the array

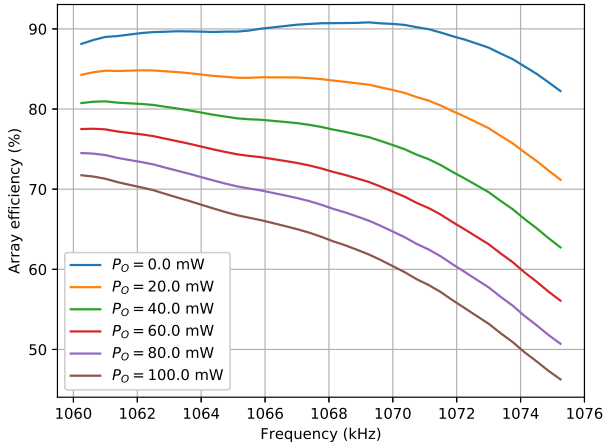

Fig. 5. Array efficiency as a function of frequency and P_O.

IV. Simulation and Experimental Results

The array performance is evaluated by a steady-state simulation using an in-house circuit simulator which is freely available at https://github.com/cechrist/cardoon. For simulations, the circuit topology is the same as shown in Fig. 2. Transducers are modelled using the measured scattering parameters in two different modes. In the first mode, the scattering parameters are only used for the fundamental frequency, for all other harmonics only the parallel capacitor of the lumped-element equivalent circuit is considered. This mode removes the odd-harmonic secondary resonances from the transducer response. In the second mode, measured S parameters are used up to the ninth harmonic. In total 4 simulations are performed for each transducer:

1) Perpendicular absorber, Mode 1
2) 45° absorber, Mode 1
3) Perpendicular absorber, Mode 2
4) 45° absorber, Mode 2

In order to experimentally verify the theory presented in this work, the six transducers were driven using the integrated driver described in [2]. Even when this driver was not originally designed for a small transducer size, it produces the same voltage and current waveforms at the transducers and therefore the experimental results can be used to determine the power delivered to the transducer and the value of δ. The effective switch capacitance, including oscilloscope probes and parasitic capacitance from PCB and connectors was experimentally determined to be 26 pF. The supply voltage was set to 20.2 V. Experimentally the output voltage was measured as the difference between the two driver outputs referred to ground. The driver was programmed to obtain duty cycles as close as possible to the values listed in Table III. The absorber was placed perpendicular to the transducer for all measurements.

Fig. 6 shows the voltage and current waves for all 4 simulations for Transducer 3. Simulations 3 and 4 clearly show that harmonic content in the current has some effect in the voltage waveform and the value of δ. However, this effect is relatively small because the charge contributions of high frequency oscillations tend to compensate each other. Figs. 7 and 8 show simulated (Simulation 3) and experimental

TABLE III
Expected performance for each transducer at 1069 kHz

Transducer	1	2	3	4	5	6
D (%)	22	22	30	29	27	19
δ	0.72	0.30	0.77	0.86	0.57	0.37
P_L (mW)	146	151	265	200	290	112
P_S (mW)	27	5	29	29	20	7

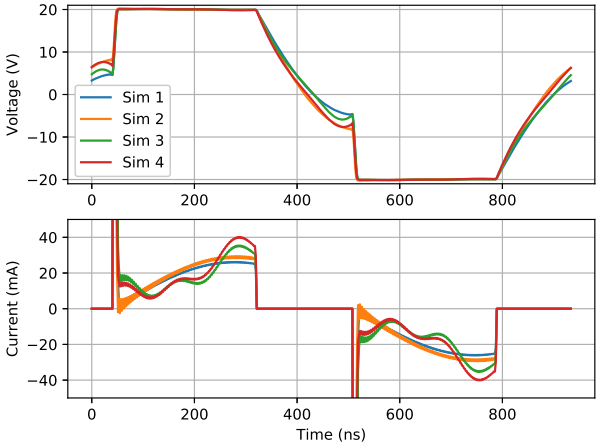

Fig. 6. Output voltage and current for Transducer 3.

transducer voltages, respectively. Overall a good agreement is observed.

Table IV and V summarize results for δ and load power

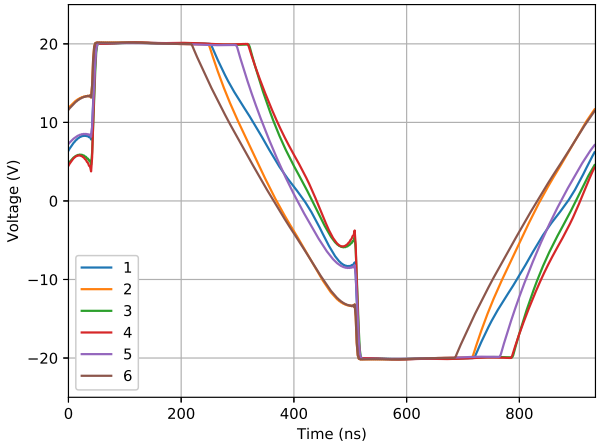

Fig. 7. Output voltage for all transducers under nominal conditions (Simulation 3).

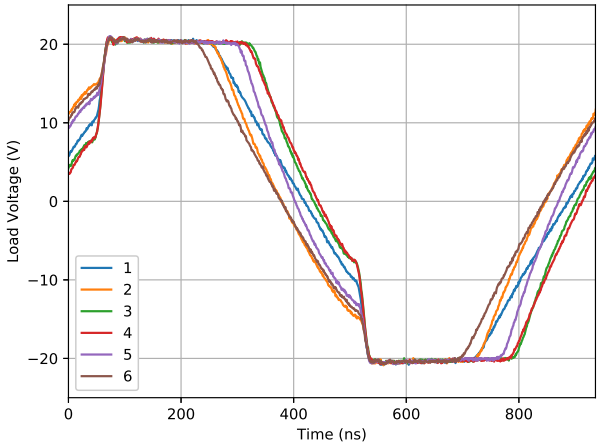

Fig. 8. Experimental output voltage for all transducers.

(P_L). For experimental results, P_L was calculated based on the measured load voltage and the measured reflection coefficient of the transducer (Γ) as follows:

$$P_L = \frac{V_o^2}{2Z_0}\frac{1-|\Gamma|^2}{|1+\Gamma|^2},$$

where V_o is determined using Fourier analysis of the sampled output voltage and Z_o is 50 Ω. Experimental results in Table IV show somewhat lower values of δ than the theory predictions in Table III, but when comparing with the values of Simulation 3, the agreement is better. These values are small enough to make switching losses a small fraction compared to the power sent to the load. The simulated results indicate that the predicted values based on the fundamental frequency response under one acoustic condition are a good approximation. Some of the differences between simulations and measurements may be due to the fact that the experimental test was performed on a different day than transducer characterization, with slightly different environmental conditions.

TABLE IV
SIMULATED AND EXPERIMENTAL δ FOR EACH TRANSDUCER AT 1069 KHZ

Transducer	1	2	3	4	5	6
Theory	0.72	0.30	0.77	0.86	0.57	0.37
Simulation 1	0.72	0.31	0.77	0.86	0.57	0.37
Simulation 2	0.68	0.30	0.60	0.82	0.57	0.32
Simulation 3	0.60	0.34	0.77	0.80	0.59	0.34
Simulation 4	0.58	0.33	0.66	0.78	0.59	0.30
Experimental	0.50	0.27	0.63	0.63	0.36	0.31

TABLE V
SIMULATED AND EXPERIMENTAL LOAD POWER (P_L) FOR EACH TRANSDUCER IN MILLIWATTS AT 1069 KHZ

Transducer	1	2	3	4	5	6
Theory	146	151	265	200	290	112
Simulation 1	143	149	258	197	282	110
Simulation 2	150	158	272	200	294	114
Simulation 3	148	145	258	199	280	110
Simulation 4	155	153	269	203	292	111
Experimental	167	160	267	201	296	118

V. CONCLUSION

This work has presented a method to determine the driving parameters to drive a piezoelectric transducer array by predicting load power and switching losses. The method was experimentally verified using a set of transducers that does not support ideal Class DE operation. This is the first work to present an approach to drive a transducer array in quasi-Class DE mode without matching networks.

ACKNOWLEDGMENT

The authors would like to thank the National Research Council of Canada (NSERC) and CMC Microsystems for supporting this work.

REFERENCES

[1] C. Christoffersen, W. Wong, S. Pichardo, G. Togtema and L. Curiel, "Class-DE Ultrasound Transducer Driver for HIFU Therapy," IEEE Transactions On Biomedical Circuits And Systems, Vol. 10, No. 2, April 2016, pp. 375-382.

[2] R. Song, C. Christoffersen, Samuel Pichardo, Laura Curiel , " An integrated full-bridge Class-DE ultrasound transducer driver for HIFU applications," *Proceedings of the 2016 IEEE NEWCAS Conference*, Vancouver, June 2016, pp. 1-4.

[3] K. Hynynen, "MRI-guided focused ultrasound treatments," *Ultrasonics*, vol. 50, no. 2, 2010, pp. 221–229.

[4] W. Wong, C. Christoffersen, Samuel Pichardo, Laura Curiel "An Integrated Ultrasound Transducer Driver For HIFU Applications," *Proc. 2013 IEEE Canadian Conf. on Electrical and Computer Engineering*, 2013, pp. 1–5.

[5] D. C. Hamill, "Impedance plane analysis of class DE amplifier," *Electronics Letters,* Vol. 30, Issue 23, pp. 1905–1906, Nov. 1994.

[6] H. Sekiya, T. Negishi, T. Suetsugu and T. Yahagi, "Operation of class DE amplifier outside optimum condition," *Proc. of IEEE ISCAS 2006*, pp. 21–24, May 2006.

[7] H. Sekiya; N. Sagawa, M. K. Kazimierczuk, "Analysis of Class-DE Amplifier With Linear and Nonlinear Shunt Capacitances at 25% Duty Ratio," *IEEE Trans on Circuits and Systems I: Regular Papers,* vol. 57, no. 9, pp. 2334–2342, 2010.